J. Phys. D: Appl. Phys. **46** (2013) 025301 (9pp) doi:10.1088/0022-3727/46/2/025301

Achieving concentrated graphene dispersions in water/acetone mixtures by the strategy of tailoring Hansen solubility parameters

Min Yi, Zhigang Shen, Xiaojing Zhang and Shulin Ma

Beijing Key Laboratory for Powder Technology Research & Development, Beijing University of Aeronautics and Astronautics, Beijing 100191, People's Republic of China

E-mail: shenzhg@buaa.edu.cn

Received 10 July 2012, in final form 13 July 2012
Published 5 December 2012
Online at stacks.iop.org/JPhysD/46/025301

Abstract

Although exfoliating graphite to give graphene paves a new way for graphene preparation, a general strategy of low-boiling-point solvents and high graphene concentration is still highly required. In this study, using the strategy of tailoring Hansen solubility parameters (HSP), a method based on exfoliation of graphite in water/acetone mixtures is demonstrated to achieve concentrated graphene dispersions. It is found that in the scope of blending two mediocre solvents, tailoring the HSP of water/acetone mixtures to approach the HSP of graphene could yield graphene dispersions at a high concentration of up to 0.21 mg ml^{-1}. The experimentally determined optimum composition of the mixtures occurs at an acetone mass fraction of ~75%. The trend of concentration varying with mixture compositions could be well predicated by the model, which relates the concentration to the mixing enthalpy within the scope of HSP theory. The resultant dispersion is highly stabilized. Atomic force microscopic statistical analysis shows that up to ~50% of the prepared nanosheets are less than 1 nm thick after 4 h sonication and 114g centrifugation. Analyses based on diverse characterizations indicate the graphene sheets to be largely free of basal plane defects and oxidation. The filtered films are also investigated in terms of their electrical and optical properties to show reasonable conductivity and transparency. The strategy of tailoring HSP, which can be easily extended to various solvent systems, and water/acetone mixtures here, extends the scope for large-scale production of graphene in low-boiling-point solutions.

(Some figures may appear in colour only in the online journal)

1. Introduction

Graphene, a two-dimensional material, has attracted considerable attention for a broad range of potential applications due to its excellent properties [1–5]. As the first step to investigate its properties and eventually to take it to real-world applications, graphene should be prepared in large quantities for large-scale applications. Various methods have been proposed to prepare graphene [6–40]. And recent developments in liquid-phase exfoliation of graphite to give graphene [6, 7, 12, 15, 17–22, 24, 25, 28–38] signify that it is possible to easily prepare low-cost graphene on a large scale for applications in electrodes, transparent films, composite formulation, surface patterning, etc.

However, there are still some problems. The liquid-phase medium used in the exfoliation process mainly includes organic solvents [19, 24, 25, 30, 35, 38], ionic liquid [17, 34], and water with surfactants or polymers as stabilizers [6, 7, 12, 18, 20–22, 29, 33, 36, 37]. On the one hand, it is difficult to remove residual surfactants [7, 12, 20, 22, 29, 33, 36, 37] or polymers [6, 18, 21] when processing graphene from water with stabilizers. On the other hand, although organic solvents such as *N*-methylpyrrolidone (NMP) can achieve high-quality graphene dispersions, they are not without

drawbacks. It has been pointed out that the best organic solvents tend to be toxic and have high boiling points [25, 28, 31, 41], making them difficult to handle during the preparation process and to remove when graphene films or composites are formed. Also, this makes it impossible to deposit individual flakes because of aggregation during the slow solvent evaporation. In addition, in order to make many applications practical, a graphene dispersion with a concentration of several hundred $\mu g\,ml^{-1}$ is required. Although some up-to-date work has reported high-concentration graphene dispersions prepared in high boiling point solvents [19, 38] and surfactant-stabilized water [20], these processes strongly rely on sonication for an extremely long time (several hundred hours), which may introduce additional defects and lower the throughput. So it would be preferable to achieve concentrated graphene dispersions in green and low-boiling-point solvents by sonication for a not very long time.

In this study, with the above-mentioned points in mind, based on the strategy of tailoring Hansen solubility parameters (HSP), we demonstrate a method to prepare concentrated graphene dispersions in water/acetone mixtures by sonication for several hours. We also noted that, some researchers recently found that graphite powders could form stable dispersion in the water/acetone mixtures [42], but they did not go further to optimize processing to achieve graphene and did not give a criterion to guide the process of producing graphene by mixing solvents. Herein, we go further to achieve high-quality concentrated graphene dispersion in water/acetone mixtures and demonstrate a HSP strategy to guide this method. Compared to the previously published work about dispersing graphite [42], the novelty of our work mainly lies in producing graphene in green low-boiling-point solvents and proposing a criterion for designing solvent mixtures to produce graphene. In our work, water and acetone are previously thought as poor solvents or nonsolvents for graphene due to their HSP mismatching those of graphene, but mixing water and acetone can tailor the solubility parameters to obtain ideal solvent systems. The optimum mixing ratio could be roughly predicted by the HSP theory. And the trend of concentration varying with mixture compositions could be predicted well by the model, which relates the concentration to the mixing enthalpy within the scope of HSP theory. Diverse characterization techniques have been used to analyse the resultant graphene and its dispersion. This method has vital advantages because water is a totally green solvent and acetone is a frequently used cheap solvent with a low boiling point of 58 °C. Because the number of solvent mixtures is limitless, the strategy of tailoring HSP allows researchers great freedom in designing ideal solvent systems for specific applications.

2. Experimental

A graphite dispersion was prepared by adding graphite (particle sizes $\leqslant$ 300 meshes) at an initial concentration of $3\,mg\,ml^{-1}$ to 30 ml water/acetone mixtures in a steel vessel with inner diameter 30 mm. A graphene dispersion was prepared by sonicating this graphite dispersion for different times (2, 4, 6, 8, 12 h), followed by centrifugation at different speeds, from 500 to 4000 rpm (36–2276g) for 30 min (Xiangyi L600). Various mixing ratios of water and acetone in mixtures were explored to find the optimum mixing ratio. For each mixing ratio, at least five samples were repeated. The steel vessel was fixed at the same position in the sonic bath (Kexi KX1620) during the whole experiment. Continuous refilling of bath water was carried out to maintain the sonication efficiency and prevent overheating. The true power output into the steel vessel was estimated to be 0.8 W by measuring the temperature rise while sonicating a known mass of water. Graphene concentration after centrifugation and standing for one week, C_G, was determined from $A/l = \alpha C_G$, where A/l was measured at 660 nm by a 721E spectrophotometer (Shanghai Spectrum) and the absorption coefficient α was determined experimentally based on Lambert–Beer behaviour. Filtered thin films with a diameter of 40 mm were prepared by vacuum filtration onto porous mixed cellulose membranes (pore size: 220 nm). These films were punched into several small circular pieces and then transferred onto glass slides with the filter membrane dissolved by acetone. After drying at 80 °C for about 120 min, the small thin films deposited on slide glasses were used for optical and electrical measurements.

UV–vis spectra of the graphene dispersion were recorded on a Purkinje General TU1901 UV–vis spectrometer. Scanning electron microscopy (SEM) images were collected by a LEO 1530VP. Atomic force microscope (AFM) images were captured with a CSPM5500 AFM (Being Nano-Instruments) in tapping mode. Bright-field transmission microscope (TEM) and high-resolution TEM (HRTEM) images were taken with a JEOL 2100 operating at 200 kV. Raman measurements were made on these films with a Renishaw Rm2000 using a 514 nm laser, where ten spectra were collected and the I_D/I_G ratio was averaged. X-ray diffraction (XRD) patterns of the filtered film were collected using Cu Kα radiation (λ = 1.5418 Å) with an x-ray diffractometer (Bruke D8-advance) operating at 40 kV and 40 mA. Fourier transformer infrared (FTIR) spectrum of the filtered film (collected as powder) was measured by a Nicolet Nexus870 spectrometer using the KBr pellet technique. X-ray photoelectron spectroscopy (XPS) investigation was performed on the filtered film dried in air by an ESCALAB-250 photoelectron spectrometer (Thermo Fisher Scientific). Optical transmission spectra of the films deposited on glass slides were recorded on a Purkinje General TU1901 UV–vis spectrometer with a glass slide as reference. Sheet resistance, R_s, was measured by a KDY-1 four-probe resistivity test system (GuangZhou KunDe).

3. Results and discussion

The absorption coefficient, α, which is related to the absorbance per unit path length, A/l, through the Lambert–Beer law $A/l = \alpha C$, is an important parameter in characterizing any dispersion. In order to accurately ascertain the graphene concentration, the absorption coefficient, α, must be determined experimentally. So we prepared a large volume of graphene dispersion in water/acetone mixtures (75 wt% acetone, which was determined as follows, 4 h sonication, 1000 rpm). Based on five graphene dispersion samples whose

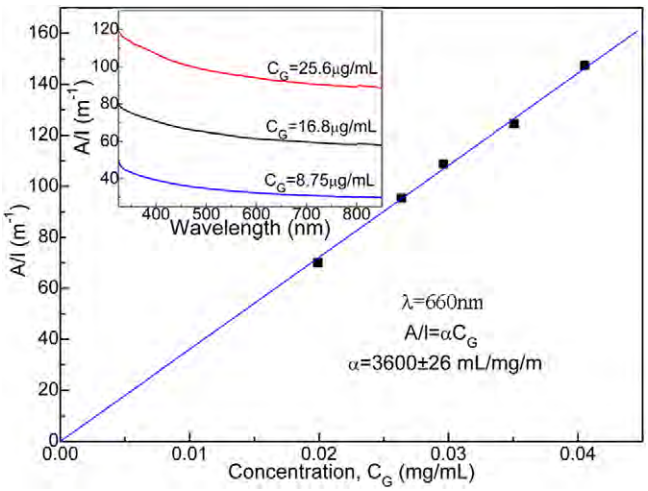

Figure 1. Absorbance per unit path length ($\lambda = 660$ nm), A/l, as a function of concentration of graphene, C_G, in water/acetone mixtures (75 wt% acetone). Lambert–Beer behaviour is shown, with an absorption coefficient $\alpha = 3600\,\mathrm{ml\,mg^{-1}\,m^{-1}}$. Inset: absorption spectra for graphene dispersed in water/acetone mixtures (75 wt% acetone) at concentrations from 8.75 to 25.6 $\mu\mathrm{g\,ml^{-1}}$.

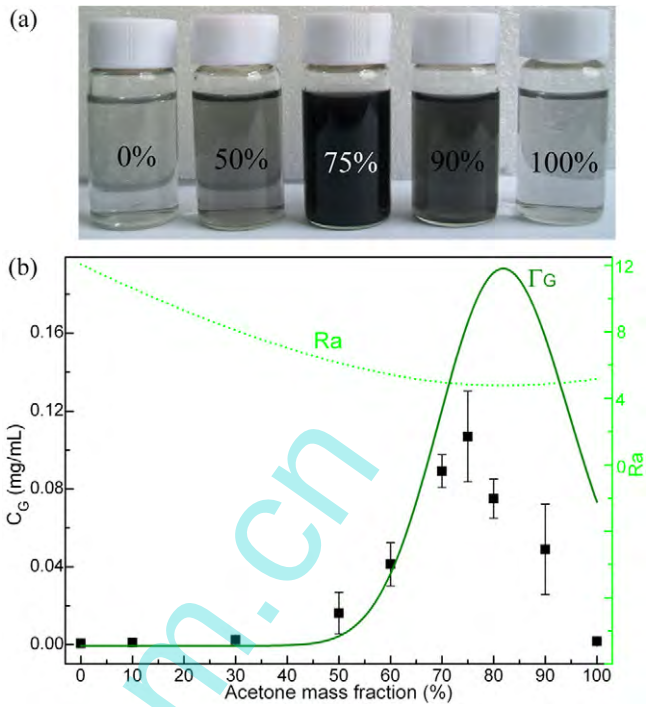

Figure 2. (*a*) Photos of graphene dispersions in various water/acetone mixtures after 4 h sonication and 1000 rpm centrifugation, which have been stored under ambient conditions for a week. (*b*) Graphene concentration, C_G, and the calculated Ra and Γ_G, as a function of the acetone mass fraction. C_G, Ra and Γ_G are shown as dots, a dotted line and a solid line, respectively.

concentrations were determined by measuring the dispersion volume and weighing the graphene film after filtration and drying, we could obtain the accurate relationship between graphene concentration, C_G, and absorbance per unit path length, A/l, as shown in figure 1. A straight line fit through these points gives an absorption coefficient at 660 nm of $\alpha = 3600\,\mathrm{ml\,mg^{-1}\,m^{-1}}$, which agrees with the reported value in high-concentration graphene dispersions [19, 38]. It should be noted that the value of α remains nearly constant regardless of the solvent composition [25]. Absorption spectra of the graphene dispersion with different concentrations were also measured (inset of figure 1). As expected for a quasi-two-dimensional material, the spectra are featureless in the visible region [43].

We optimized the mixing ratio of water and acetone by measuring the concentration (proportional to A/l) of graphene remaining dispersed after sonication and centrifugation as a function of acetone mass fraction (4 h sonication, 1000 rpm). It has been proved that the rotation rates of 25g was the minimum required to remove large aggregates, while the rotation rates of more than 400g could result in graphene with considerable body defects [20]. Thus, we chose an interval value, 1000 rpm (144g), to obtain a graphene dispersion. The results are shown in figure 2, where the graphene concentration highly depends on the acetone mass fraction. Appreciable discrepancies of graphene concentration under different mixing ratios are clear to the naked eye, as presented in figure 2(*a*). Pure water and pure acetone produce only an almost transparent dispersion, while at an appropriate acetone mass fraction a dark black graphene dispersion can be obtained. From figure 2(*b*), it can be seen that the maximum graphene concentration occurs at an acetone mass fraction of ∼75%, which can be taken as the optimum mixing ratio. The maximum graphene concentration during centrifugation of 1000 rpm reaches $\sim 0.11\,\mathrm{mg\,ml^{-1}}$, which is several hundred times higher than that in pure water or acetone. This maximum graphene concentration of $\sim 0.11\,\mathrm{mg\,ml^{-1}}$, achieved in the water/acetone mixtures, is comparable to the previously reported maximum values in NMP [19] and sodium cholate stabilized water [20]. However, those reported high-concentration graphene dispersions were achieved by sonication for several hundred hours [19, 20].

As for the theoretical considerations of optimizing the mixing ratio, we turn to the HSP theory [44, 45]. It has been evidenced that good solvents should have HSP matching those of graphene [28, 31, 41]. And blending two mediocre solvents, water and acetone, can tailor the solubility parameters of the mixtures to approach the HSP of graphene [44, 45]. According to Hansen, each solvent or material has three Hansen parameters: δ_D, δ_P and δ_H, which can be located in the 3D Hansen space just as co-ordinates [44, 45]. In the Hansen space, between solvent 1 and solute 2, HSP distance Ra is defined as $\mathrm{Ra} = (4(\delta_{D1}-\delta_{D2})^2+(\delta_{P1}-\delta_{P2})^2+(\delta_{H1}-\delta_{H2})^2)^{1/2}$. Hence the idea is the smaller the Ra, the higher the solubility [44, 45]. Additionally, the HSP of a mixture is proportional to the volume fractions of its component solvents [44, 45]. So for the water/acetone mixtures here, $\delta_{i,\mathrm{mix}} = ((1-\phi_a)/\rho_w\delta_{i,w} + \phi_a/\rho_a\delta_{i,a})/((1-\phi_a)/\rho_w + \phi_a/\rho_a)$, where i denotes D, P or H, ϕ_a denotes the acetone mass fraction, ρ_w and ρ_a denote the density of water and acetone, respectively. Based on the HSP of graphene [41], which has been estimated as $\delta_{D,G} \sim 18\,\mathrm{MPa^{1/2}}$, $\delta_{P,G} \sim 9.3\,\mathrm{MPa^{1/2}}$ and $\delta_{H,G} \sim 7.7\,\mathrm{MPa^{1/2}}$, and the HSP of water [45] ($\delta_D \sim 18.1\,\mathrm{MPa^{1/2}}$, $\delta_P \sim 17.1\,\mathrm{MPa^{1/2}}$ and $\delta_H \sim 16.9\,\mathrm{MPa^{1/2}}$, correlation with total miscibility) and acetone [45] ($\delta_D \sim 15.5\,\mathrm{MPa^{1/2}}$, $\delta_P \sim 10.4\,\mathrm{MPa^{1/2}}$ and $\delta_H \sim 7\,\mathrm{MPa^{1/2}}$), Ra between graphene and the water/acetone

mixture can be calculated, as shown by the dotted line in figure 2(*b*). It can be seen that the smallest Ra occurs around the highest concentration. However, it should be noted that Ra here has a very broad minimum in the 60–90% range. In this broad range, it is strange that such small changes in Ra surprisingly lead to such a sharp change in the solubility of graphene. This phenomenon cannot be explained perfectly in the scope of Ra. Hence, we further try a more sophisticated model within the HSP theory, relating mixing enthalpy to graphene concentration. It has been proposed that, similar to the case of nanotube, the dispersion concentration of graphene, Ω_G, can be given by [28]

$$\Omega_G \propto \exp\left[-\frac{\bar{v}}{RT}\frac{\partial(\Delta H/V)}{\partial\varphi}\right],$$

where $\bar{v}$ is the molar volume of graphene which is a constant, $\Delta H/V$ is the enthalpy of mixing per volume of the mixture (graphene and solvents), φ is the dispersed graphene volume fraction. According to Hansen [44, 45], the enthalpy of mixing can be written as

$$\frac{\Delta H}{V} \approx \varphi(1-\varphi)\left[(\delta_{D,mix}-\delta_{D,G})^2+\frac{1}{4}(\delta_{P,mix}-\delta_{P,G})^2 + \frac{1}{4}(\delta_{H,mix}-\delta_{H,G})^2\right].$$

Considering that the volume fraction of dispersed graphene is very low ($1-\varphi \approx 1$) and $\bar{v}/RT$ remains constant, we can obtain that

$$\Omega_G \propto \Gamma_G = \exp[-(\delta_{D,mix}-\delta_{D,G})^2 - \tfrac{1}{4}(\delta_{P,mix}-\delta_{P,G})^2 - \tfrac{1}{4}(\delta_{H,mix}-\delta_{H,G})^2].$$

Thus, we can plot the relationship between Γ_G and acetone mass fraction, as shown by the solid line in figure 2(*b*). Obviously, in the scope of Γ_G, the predicted trend of concentration varying with acetone mass fraction agrees better with the experimental data. So it can be concluded that by tailoring the HSP of the water/acetone mixtures to approach the HSP of graphene, mixing water and acetone can yield concentrated graphene dispersions. And the trend of concentration varying with mixture compositions could be well predicated by the model which relates the concentration to the mixing enthalpy within the scope of HSP theory. Based on the above discussion, we can deduce that the physical origin of our results lies in that: mixing blending two mediocre solvents (for example, water and acetone used here) can tailor the HSP of mixed solvents to approach the HSP of graphene, thus minimizing the enthalpy of mixing and obtaining concentrated and stable graphene dispersion.

We also investigated the stability of the prepared graphene dispersions at the optimum mixing ratio by monitoring the dispersion concentration optically. Typical sedimentation curves for graphene dispersed in the water/acetone mixtures are plotted in figure 3 (75 wt% acetone, 4 h sonication, the dispersion centrifuged at 1000 rpm, 2000 rpm and 4000 rpm was diluted by factors of 6, 3 and 2, respectively). The investigated sample is very stable over one month, showing <22% sedimentation. It was verified that during sedimentation

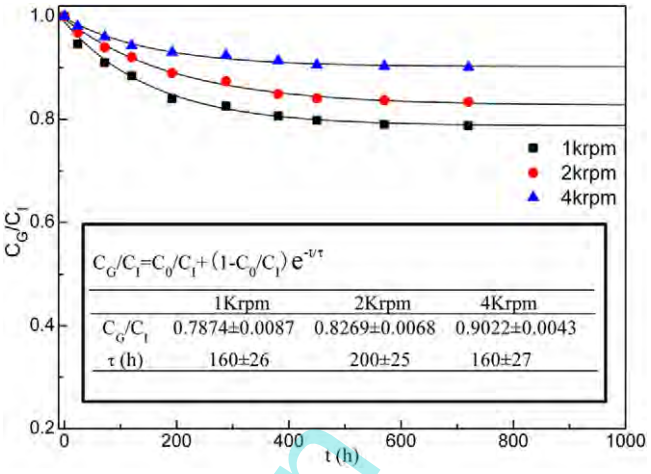

Figure 3. Sedimentation curves for graphene dispersed in water/acetone mixtures (75 wt% acetone) after 4 h sonication and 1000, 2000 and 4000 rpm centrifugation. Inset: the equation based on which the plotted solid lines are fitted, where C_G/C_I is the concentration normalized to the total initial concentration. The fitting results are also presented in the inset.

the concentration, C_G, can be approximately fitted by the inset equation of figure 3, $C_G/C_I = C_0/C_I + (1-C_0/C_I)e^{-t/\tau}$, where C_0 is the concentration of the stable phase, $(C_I - C_0)$ is the concentration of the sedimenting phase and τ is the time constant. The fitting results for 1000 rpm centrifugation are characterized by $C_0/C_I \sim 79\%$ and $\tau \sim 160$ h, indicating considerable stability, which are comparable to the stability in good solvents such as *N*-methylpyrrolidone [25].

Moreover, we explored the effect of sonication time (t_s) and centrifugation speed (ω) on the graphene concentration in the optimum water–acetone mixture. As shown in figure 4(*a*), the concentration increases with sonication time, reaching a value of $\sim$0.21 mg ml^{-1} when $t_s = 12$ h. Apparently, within the short sonication time ($\leqslant$12 h) in this study, C_G in figure 4(*a*) approximately scales linearly with t_s. But it can be anticipated that as t_s increases to a certain value, C_G may approach saturation. Meanwhile, in figure 4(*b*) as centrifugation speed (ω) increases, C_G decreases from $\sim$0.21 mg ml^{-1} at 500 rpm to $\sim$0.03 mg ml^{-1} at 4000 rpm. By fitting C_G as a function of ω, it can be seen that C_G scales with ω^{-1}.

Furthermore, we performed AFM, TEM, XRD, FTIR, Raman spectrum and XPS analyses to evaluate the quality of the dispersion. It should be noted that we have tried to distinguish the distribution of layer number and lateral size of graphene flakes prepared in different mixture compositions, ω and t_s based on TEM and AFM, but no firm evidence and regular results were obtained. Generally, only extremely small portions of thousands of graphene flakes in one dispersion sample were captured by AFM and TEM. So the sample volume used in the quantitative analysis based on AFM and TEM was too small to reach a solid conclusion. Hence, the differences between individual graphene flakes in different mixture compositions, ω and t_s will not be addressed in this study. Nevertheless, the results from AFM and TEM are widely used as important references for evaluating the dispersion quality. In the following, we choose the dispersion

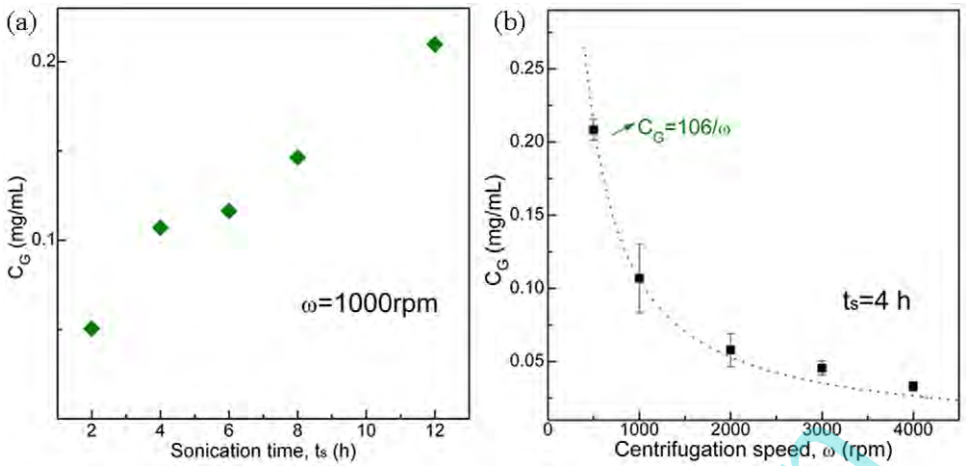

Figure 4. C_G in the optimum mixture as functions of (*a*) sonication time and (*b*) centrifugation speed.

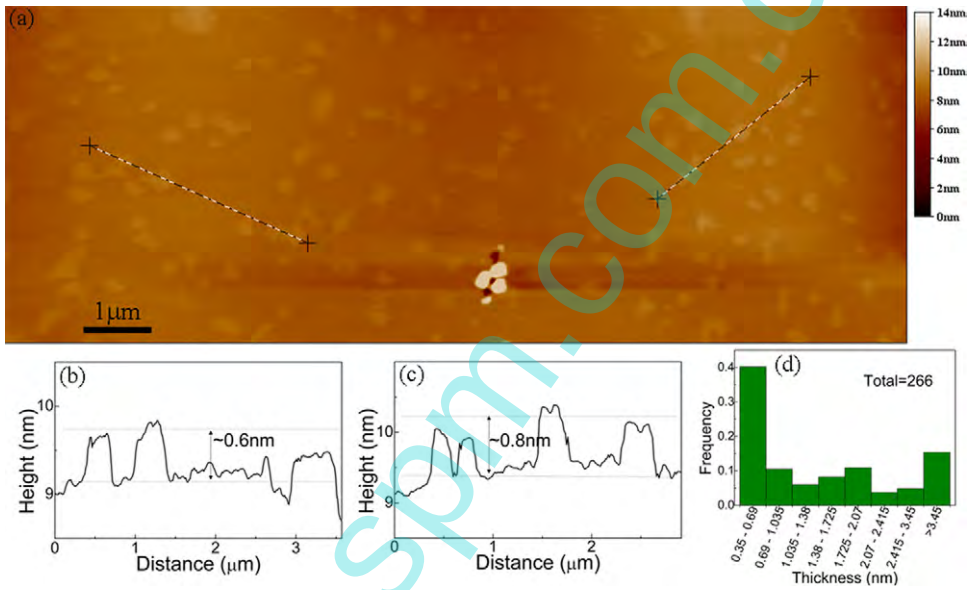

Figure 5. (*a*) A typical AFM image showing a large number of individual graphene flakes due to the low boiling point of acetone and water. (*b*), (*c*) Section analysis of the left line and right line in (*a*), respectively. (*d*) A histogram of the frequency of nanosheets captured by AFM as a function of the thickness per nanosheet in the water/acetone dispersion.

prepared in the optimum mixture with $t_s = 4$ h and $\omega = 1000$ rpm to perform all these characterizations. Figures 5 and 6 present typical AFM and TEM images of graphene flakes in the optimum mixture (75 wt% acetone, $t_s = 4$ h, $\omega = 1000$ rpm). The low boiling point of water and acetone allowed individual flakes to easily spray-cast onto the mica substrates. In AFM images, numerous individual graphene flakes of several hundred nanometres length and <1 nm thickness were captured, as shown in figure 5(*a*). Two cross sections in figure 5(*a*) show height steps of ~0.6 nm (figure 5(*b*)) and ~0.8 nm (figure 5(*c*)), indicating monolayers or at most bilayer flakes. Based on more than 200 flakes captured by AFM, a statistical analysis of height distribution can be obtained from figure 5(*d*). It has been demonstrated that due to some external factors from the AFM instrument and substrates [11, 46], monolayer graphene is often measured as 0.4–1 nm thick by AFM. Thus, from figure 5(*d*), it can be estimated that almost 50% of graphene flakes are monolayers. An optimum value of ω can hardly be obtained in this study. But in view of the reported result that a suitable rotation rate is between 25g and 400g [20], the AFM results of 50% flakes as monolayers indicate that 1000 rpm (114g) in this study is enough to remove large and thick flakes and obtain a graphene dispersion with relatively high quality.

Representative TEM and HRTEM images are shown in figure 6. The graphene flakes captured by TEM are of lateral size of several micrometres, often larger than those captured by AFM. This could be attributed to the fact that the smaller flakes may be lost through the holes in the grid used for TEM samples. Figure 6(*d*) shows graphene flakes which are folded and piled. When paying attention to the protruding flake, as indicated by a circle in figure 6(*d*), a HRTEM image can be obtained in figure 6(*e*). The fast Fourier transform (FFT) image (inset of figure 6(*e*)) of figure 6(*e*), which is equivalent to a diffraction pattern, shows a bright inner ring of {1 1 0 0} spots and an extremely faint outer ring of {2 1 1 0} spots, as

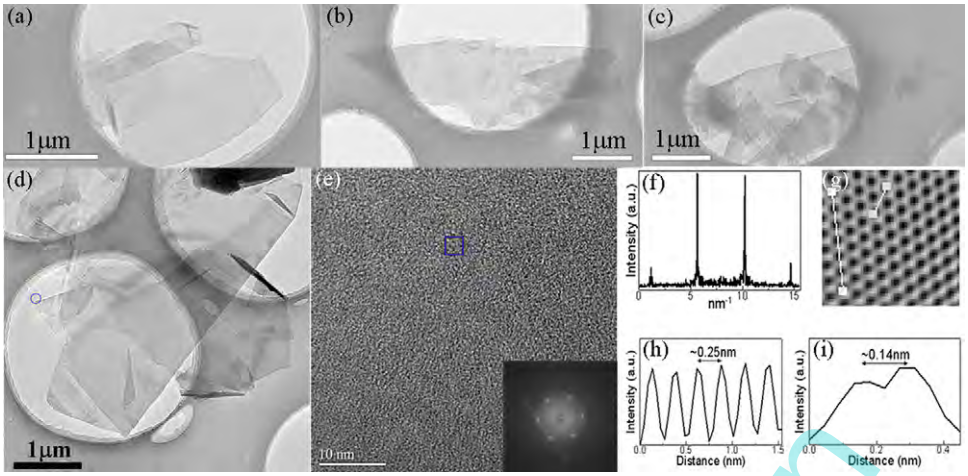

Figure 6. (*a*)–(*c*) Some representative bright-field TEM images of graphene flakes. (*d*) A typical TEM image of several folded and piled graphene flakes prepared in the water/acetone mixtures. (*e*) A HRTEM image of a section of a graphene monolayer which protrudes at an edge of the flakes in (*d*), as indicated by a circle in (*d*). Inset: FFT image of (*e*), which is equivalent to an electron diffraction pattern. (*f*) Intensity distribution of spots in the rectangle in the inset FFT of (*e*). (*g*) A filtered image (Fourier mask filtering, twin-oval patter, edge smoothed by five pixels) of part of the square in (*e*). (*h*) Intensity analysis along the left line in (*g*) shows a hexagon width of ∼0.25 nm. (*i*) Intensity analysis along the right line in (*g*) shows a C–C bond length of ∼0.14 nm.

exhibited in figure 6(*f*). So the FFT here reveals the typical diffractions of the monolayer [25, 33, 36], signifying that the region indicated by a circle in figure 6(*d*) is a monolayer. A filtered image of the square in figure 6(*e*) is presented in figure 6(*g*), which clearly displays the hexagonal atomic skeleton of graphene. Moreover, intensity analysis along the line in figure 6(*g*) illustrates a hexagon width of ∼0.25 nm (figure 6(*h*)), close to the theoretical value of 2.5 Å, and gives a C–C bond length of ∼0.14 nm (figure 6(*i*)), coinciding with the expected value of 1.42 Å. In addition, all imaged regions exhibit a structure similar to this, indicating defect-free graphene and a nondestructive method.

In order to consider the structure and defect information of the exfoliated graphene, we measured XRD, FTIR, Raman spectrum and XPS of the thin films formed by vacuum filtration of the graphene dispersion. Figure 7 shows the representative XRD and FTIR spectra for the samples. In figure 7(*a*), the peak position in the filtered film corresponding to the (0 0 2) plane is almost identical to those in pristine graphite. This indicates that the graphite lattice parameters remain and the crystal structure is not destroyed. However, no (0 0 4) peak is observed for the filtered film. Hence, the sublattices in the filtered film are almost completely devoid of long-range order greater than four layers [47]. Additionally, it has been known that the shear force and shock waves created by sonication-induced cavitation bubbles can exfoliate pristine graphite into smaller and thinner flakes [36, 48, 49], as shown in figures 7(*b*) and (*c*). As a consequence, the relative intensity of the (0 0 2) peak is remarkably decreased from the pristine graphite case and the FWHM of the (0 0 2) peak is increased from 0.199° to 0.374° due to Scherrer broadening [50, 51].

The FTIR spectrum in figure 7(*d*) shows peaks around 1560 cm^{-1}, which are assigned to the stretching of C=C bonds of graphitic domains, and around 3430 cm^{-1}, which is due to the stretching vibration of water molecules in KBr.

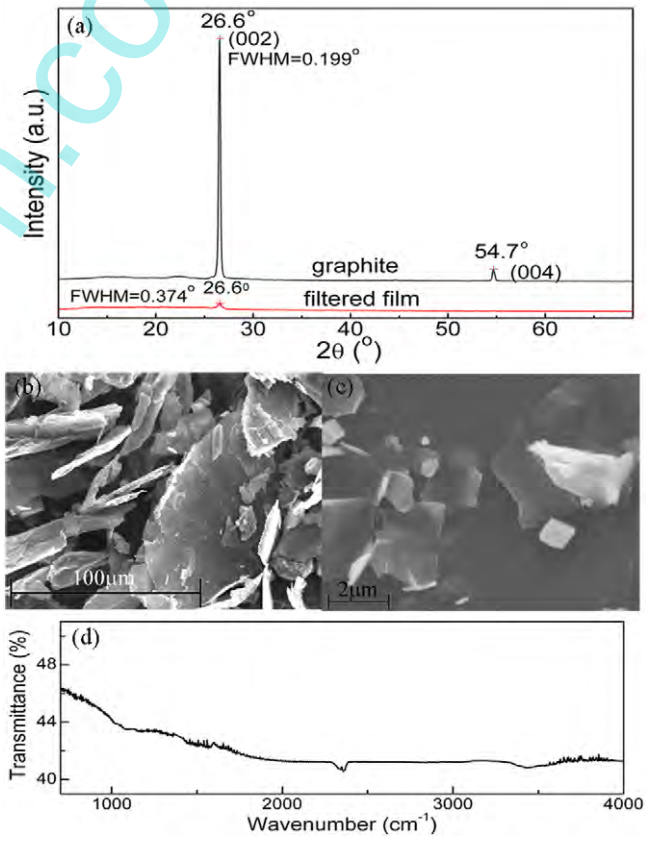

Figure 7. (*a*) XRD spectra of pristine graphite and the film filtered from the graphene dispersion after 1000 rpm centrifugation. (*b*) A SEM image of graphite flakes before sonication. (*c*) A SEM image of graphite flakes after sonication recovered as a precipitate after 1000 rpm centrifugation. (*d*) FTIR spectrum of graphene powders (collected from films filtered from the graphene dispersion after 1000 rpm centrifugation) in a KBr pellet.

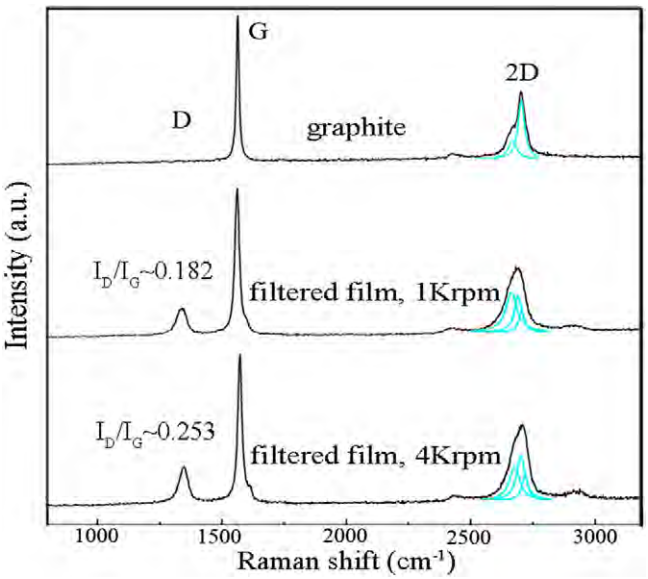

Figure 8. Typical Raman spectra of graphite and films filtered from graphene dispersion after 1000 and 4000 rpm centrifugation. The intensity was normalized by the G peak and the values of I_D/I_G were calculated by averaging ten spectra collected in one film. The 2D bands ($\sim 2700\,\mathrm{cm}^{-1}$) are fitted by Lorentz functions.

Most importantly, the spectrum in figure 7(*d*) shows no peaks associated with C–OH ($\sim$1340 cm^{-1}) and –COOH ($\sim$1710–1720 cm^{-1}) groups. This result is entirely different from the films made from reduced graphene oxide (GO) or chemically derived graphene [52–55], further proving that the method here does not chemically functionalize the prepared graphene and that we produce graphene rather than some form of graphene derivatives.

The defect content of the exfoliated graphene was also considered by Raman spectrum. Examples of typical film spectra are given in figure 8, alongside a spectrum for pristine graphite (these spectra were normalized to the intensity of the G band at $\sim$1582 cm^{-1}). Spectra of graphitic materials are characterized by a D-band ($\sim$1350 cm^{-1}), a G-band ($\sim$1582 cm^{-1}) and a 2D-band ($\sim$2700 cm^{-1}) [56, 57]. The shape of 2D band is indicative of the number of monolayers per graphene flake. So we firstly look at this band. We have fitted the 2D bands of pristine graphite and films filtered from graphene dispersion by using Lorentz functions, as shown in figure 8. According to the literature about relationships between layer number and Lorentz function-based fitting components of 2D bands [25, 56, 57], we can see from figure 8 that the 2D bands of the filtered films present the evidence of graphene flakes no more than 5 layers [25, 56, 57]. It should be noted that our Raman spectrum analyses were within the scope of films filtered from graphene dispersion. So the 2D bands also give information about the films which could be taken as a whole. Apparently, the 2D bands in the filtered films are distinct from 2D band in pristine graphite, indicating the nature of few-layer graphene [25, 56, 57]. This indicates that though aggregation of graphene flakes happens during the filtration, the aggregation is not a process to drive graphene flakes stacked in Bernal AB style which exists in graphite. Therefore, the filtered film from graphene dispersion is neither graphene nor graphite, but a randomly stacked graphene block of numerous graphene flakes. The defect content can be characterized by the intensity of the D band relative to the G band, I_D/I_G. We note that spectra in the filtered films have D bands significantly larger than those of the starting powder, indicating that the preparation process induces defects. Such defects can be divided into two main types: basal plane defects and edge defects. Basal plane defects can generally result in an obvious broadening of G bands, which is often found in chemically reduced graphene [25, 58, 59]. The introduction of edge defects is unavoidable, because cavitation-induced shear force and shock waves cut the initial large crystallite into smaller flakes and the dynamic flow during the vacuum filtration may tear or fold micrometre sheets into submicrometre ones [36, 48, 49]. These smaller flakes in the filtered films have more edges per unit mass, so that increases the content of edge defects. Consequently, seeing that the broadening of G band is unremarkable and the size of the laser point (1–2 μm) used in the Raman system will inevitably cover the edges of the graphene sheets in the filtered film, the D band in the filtered film may be largely attributed to the edge defects instead of the basal plane defects. Also, the intensity ratio of I_D/I_G for the filtered film is less than 0.253, which is much lower than that of the GO and chemically reduced graphene [58, 59].

The best evidence for the presence of defects in the form of oxides can be obtained by XPS, a surface-sensitive technique that probes the top 3–4 nm of a material sample [60]. Based on the XPS survey spectra in figure 9(*a*), it can be seen that the composition of the filtered film (C $\sim$ 94.9% and O $\sim$ 5.1%) is similar to the composition of pristine graphite (C $\sim$ 96.0% and O $\sim$ 4.0%). Figure 9(*b*) summarizes the results of the C1s XPS spectrum of pristine graphite and the filtered film. Both XPS spectra show the most dominant peaks around 284.8 eV (C–C), accompanied by two small additional fitting-determined peaks around 285.7 and 286.8 eV, which correspond to the following carbon components: C–OH and C=O [61, 62]. It should be noted that in contrast to GO or chemically reduced GO [61], the peak around 288.7 eV corresponding to O=C–OH is not presented, further indicating unobservable oxidation. Additionally, the oxides of pristine graphite are often observed due to chemi- and physisorbed water, CO_2 or oxygen [63]. In view of the same bonds and similar composition in the pristine graphite and filtered film, it can be deduced that the low level of oxides in graphene is caused not by residual solvent but by water, CO_2 or oxygen from the atmosphere. Combining the Raman, FTIR and XPS results, we can conclude that the graphene prepared here is largely free of basal plane defects and oxidation, residual solvent is nearly absent even under air drying at room temperature, and our method is mild.

To test the optical and electrical properties of the filtered films, we measured the transmittance spectrum and sheet resistance of the film transferred from the cellulose membrane to the slide glass. The estimated thickness of the deposited film was calculated by $t = m/\rho A$, where m is the film mass given by dispersion volume multiplied by concentration, ρ is the film density taken as 2.2 g cm^{-3} and A is the area of the Ø40 mm film [12]. Hence, the thickness of the measured film can be estimated to be $\sim$100 nm. The transmittance spectrum

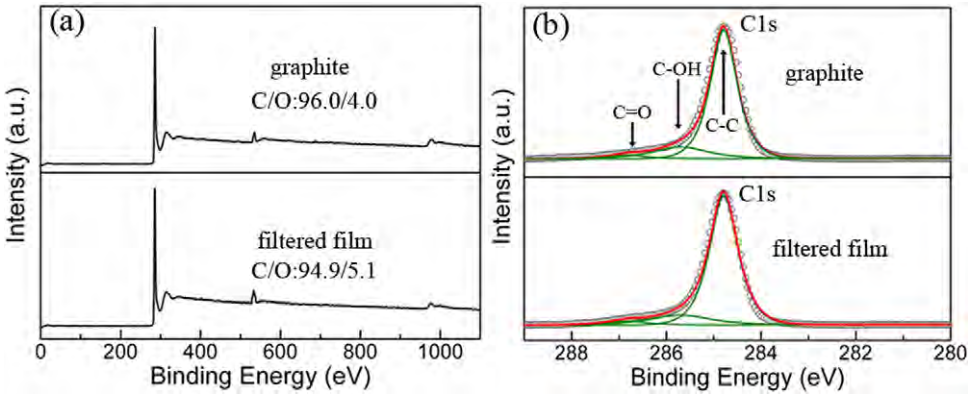

Figure 9. (*a*) XPS survey spectra and (*b*) C1s XPS spectra of pristine graphite and the film filtered from the graphene dispersion after 4 h sonication and 1000 rpm centrifugation.

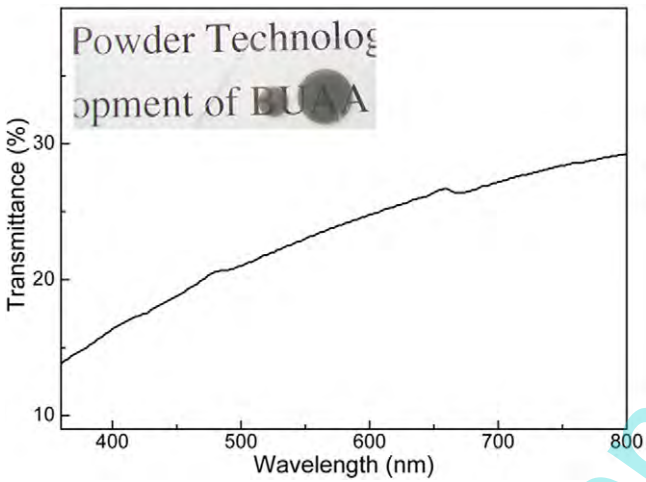

Figure 10. Transmittance spectra of thin films of estimated thickness ~100 nm. Upper left inset photo shows the film on the glass slide substrate.

and the photograph of the thin film are presented in figure 10. The sheet resistance, R_s, was measured to be ~10 kΩ/□ and the transmittance at 550 nm to be ~23%. This corresponds to a dc conductivity of ~1000 S m^{-1}. This value is higher than the reported value of unannealed films made from surfactant-stabilized dispersions [29]. The moderate conductivity value is probably attributed to the film transfer process from the filter membrane to the glass slide; because we measured the film directly deposited on the filter membrane and found a sheet resistance of ~240 Ω/□ (~4.2×10^4 S m^{-1}). However, we believe that the combination of low boiling point of water and acetone, and lack of defects gives our water/acetone mixture based exfoliation method great potential. In future studies, we will focus on improving the thin film deposition and transfer process to maximize the electrical conductivity of the films deposited on various transparent substrates.

4. Conclusions

In conclusion, based on the strategy of tailoring HSP, we demonstrated a method to achieve high-concentration graphene dispersions by tailoring the HSP of a mixture of water and acetone. By altering the composition of water/acetone mixtures, the HSP of the mixture can be tailored to approach that of graphene based on the HSP theory. The mixture with an optimum acetone mass fraction of 75%, which is consistent with the HSP theory prediction, could achieve a 0.21 mg ml^{-1} graphene dispersion by mild sonication for 12 h. The trend of concentration varying with mixture compositions could be predicted well by the model, which relates the concentration to the mixing enthalpy within the scope of HSP theory. The dispersion is highly stabilized in the mixtures, which are comparable to the stability in good solvents such as *N*-methylpyrrolidone. AFM statistical analysis indicates that graphene flakes of less than 1 nm thickness occupy ~50%. HRTEM, FTIR, XRD, Raman spectrum and XPS analyses manifest that the graphene flakes prepared here are largely free of basal defect and oxidation. Thin films, which can be deposited on transparent glass substrates by vacuum filtration and transfer process, are reasonably conductive and can be made semitransparent. It is anticipated that the optical electrical properties can be considerably improved by optimizing the formation process of thin films. Our method shows vital advantages for low-boiling-point solvents and will extend the scope for efficient large-scale production of graphene in low-boiling-point solutions. In addition, seeing that the number of solvent mixtures is limitless, the available solvents are not limited to water and acetone. The strategy of tailoring HSP can be easily extended to various solvent systems, and allows researchers great freedom in designing ideal solvent systems for preparation and specific applications of graphene.

Acknowledgments

This works was funded by the financial support from the Special Funds for Co-construction Project of the Beijing Municipal Commission of Education, the '985' Project of the Ministry of Education of China and the Fundamental Research Funds for the Central Universities.

References

[1] Zhu Y, Murali S, Cai W, Li X, Suk J W, Potts J R and Ruoff R S 2010 *Adv. Mater.* **22** 3906

[2] Geim A K 2009 *Science* **324** 1530
[3] Wu J, Pisula W and Mullen K 2007 *Chem. Rev.* **107** 718
[4] Allen M J, Tung V C and Kaner R B 2010 *Chem. Rev.* **110** 132
[5] Geim A K and Novoselov K S 2007 *Nature Mater.* **6** 183
[6] Bourlinos A B, Georgakilas V, Zboril R, Steriotis T A, Stubos A K and Trapalis C 2009 *Solid State Commun.* **149** 2172
[7] Vadukumpully S, Paul J and Valiyaveettil S 2009 *Carbon* **47** 3288
[8] Park S and Ruoff R S 2009 *Nature Nanotechnol.* **4** 217
[9] Loh K P, Bao Q, Ang P K and Yang J 2010 *J. Mater. Chem.* **20** 2277
[10] Dreyer D R, Park S, Bielawski C W and Ruoff R S 2010 *Chem. Soc. Rev.* **39** 228
[11] Novoselov K S, Geim A K, Morozov S V, Jiang D, Zhang Y, Dubonos S V, Grigorieva I V and Firsov A A 2004 *Science* **306** 666
[12] De S, King P J, Lotya M, O'Neill A, Doherty E M, Hernandez Y, Duesberg G S and Coleman J N 2010 *Small* **6** 458
[13] Norimatsu W, Takada J and Kusunoki M 2011 *Phys. Rev.* B **84** 035424
[14] Choucair M, Thordarson P and Stride J A 2009 *Nature Nanotechnol.* **4** 30
[15] Inagaki M, Kim Y A and Endo M 2011 *J. Mater. Chem.* **21** 3280
[16] Sun Z, Yan Z, Yao J, Beitler E, Zhu Y and Tour J M 2010 *Nature* **468** 549
[17] Nuvoli D, Valentini L, Alzari V, Scognamillo S, Bon S B, Piccinini M, Illescas J and Mariani A 2011 *J. Mater. Chem.* **21** 3428
[18] Liu Y-T, Xie X-M and Ye X-Y 2011 *Carbon* **49** 3529
[19] Khan U, O'Neill A, Lotya M, De S and Coleman J N 2010 *Small* **6** 864
[20] Lotya M, King P J, Khan U, De S and Coleman J N 2010 *ACS Nano* **4** 3155
[21] Liang Y T and Hersam M C 2010 *J. Am. Chem. Soc.* **132** 17661
[22] Guardia L, Fernández-Merino M J, Paredes J I, Solís-Fernández P, Villar-Rodil S, Martínez-Alonso A and Tascón J M D 2011 *Carbon* **49** 1653
[23] Tung V C, Allen M J, Yang Y and Kaner R B 2009 *Nature Nanotechnol.* **4** 25
[24] Hamilton C E, Lomeda J R, Sun Z, Tour J M and Barron A R 2009 *Nano Lett.* **9** 3460
[25] Hernandez Y *et al* 2008 *Nature Nanotechnol.* **3** 563
[26] Li X *et al* 2009 *Science* **324** 1312
[27] Kim K S, Zhao Y, Jang H, Lee S Y, Kim J M, Ahn J H, Kim P, Choi J Y and Hong B H 2009 *Nature* **457** 706
[28] Coleman J N 2012 *Acc. Chem. Res.* doi: 10.1021/ar300009f
[29] Lotya M *et al* 2009 *J. Am. Chem. Soc.* **131** 3611
[30] Bourlinos A B, Georgakilas V, Zboril R, Steriotis T A and Stubos A K 2009 *Small* **5** 1841
[31] Coleman J N 2009 *Adv. Funct. Mater.* **19** 3680
[32] Cui X, Zhang C, Hao R and Hou Y 2011 *Nanoscale* **3** 2118
[33] Yi M, Li J, Shen Z, Zhang X and Ma S 2011 *Appl. Phys. Lett.* **99** 123112
[34] Lu J, Yang J X, Wang J, Lim A, Wang S and Loh K P 2009 *ACS Nano* **3** 2367
[35] Zhao W, Fang M, Wu F, Wu H, Wang L and Chen G 2010 *J. Mater. Chem.* **20** 5817
[36] Shen Z, Li J, Yi M, Zhang X and Ma S 2011 *Nanotechnology* **22** 365306
[37] Knieke C, Berger A, Voigt M, Taylor R N K, Röhrl J and Peukert W 2010 *Carbon* **48** 3196
[38] Khan U, Porwal H, O'Neill A, Nawaz K, May P and Coleman J N 2011 *Langmuir* **27** 9077
[39] Behabtu N *et al* 2010 *Nature Nanotechnol.* **5** 406
[40] Lee S, Lee K and Zhong Z 2010 *Nano Lett.* **10** 4702
[41] Hernandez Y, Lotya M, Rickard D, Bergin S D and Coleman J N 2010 *Langmuir* **26** 3208
[42] Nonomura Y, Morita Y, Deguchi S and Mukai S 2010 *J. Colloid Interface Sci.* **346** 96
[43] Abergel D S L and Fal'ko V I 2007 *Phys. Rev.* B **75** 155430
[44] Abbott S, Hansen C M and Yamamoto H 2010 *Hansen Solubility Parameters in Practice* (Hørsholm, Denmark: Hansen-Solubility)
[45] Hansen C M 2007 *Hansen Solubility Parameters: A User's Handbook* (Boca Raton, FL: CRC Press)
[46] Nemes-Incze P, Osváth Z, Kamarás K and Biró L P 2008 *Carbon* **46** 1435
[47] Shih C J *et al* 2011 *Nature Nanotechnol.* **6** 439
[48] Suslick K S and Price G J 1999 *Annu. Rev. Mater. Sci.* **29** 295
[49] Cravotto G and Cintas P 2010 *Chem.-Eur. J.* **16** 5246
[50] Morant R A 1970 *J. Phys. D: Appl. Phys.* **3** 1367
[51] Wilson N R *et al* 2009 *ACS Nano* **3** 2547
[52] Li X, Zhang G, Bai X, Sun X, Wang X, Wang E and Dai H 2008 *Nature Nanotechnol.* **3** 538
[53] Whitby R L D, Korobeinyk A, Mikhalovsky S V, Fukuda T and Maekawa T 2011 *J. Nanopart. Res.* **13** 4829
[54] Li D, Muller M B, Gilje S, Kaner R B and Wallace G G 2008 *Nature Nanotechnol.* **3** 101
[55] Si Y and Samulski E T 2008 *Nano Lett.* **8** 1679
[56] Malard L M, Pimenta M A, Dresselhaus G and Dresselhaus M S 2009 *Phys. Rep.* **473** 51
[57] Ferrari A C *et al* 2006 *Phys. Rev. Lett.* **97** 187401
[58] Stankovich S, Piner R D, Chen X, Wu N, Nguyen S T and Ruoff R S 2006 *J. Mater. Chem.* **16** 155
[59] Stankovich S, Dikin D A, Piner R D, Kohlhaas K A, Kleinhammes A, Jia Y, Wu Y, Nguyen S T and Ruoff R S 2007 *Carbon* **45** 1558
[60] Briggs D and Seah M P 1996 *Practical Surface Analysis, Auger and X-ray Photoelectron Spectroscopy* (New York: Wiley)
[61] Yang D *et al* 2009 *Carbon* **47** 145
[62] Polyakova E Y, Rim K T, Eom D, Douglass K, Opila R L, Heinz T F, Teplyakov A V and Flynn G W 2011 *ACS Nano* **5** 6102
[63] Wu Y, Jiang C, Wan C and Holze R 2002 *J. Power Sources* **111** 329